

**Diagnostic Evaluation of Ozone Production and Horizontal Transport
in a Regional Photochemical Air Quality Modeling System**

James M. Godowitch^{a*}, Robert C. Gilliam^a, S.Trivikrama Rao^a

^aAtmospheric Modeling and Analysis Division, National Exposure Research Laboratory
Office of Research and Development, U.S. Environmental Protection Agency
Research Triangle Park, NC 27711 USA

* *Corresponding author address.* James Godowitch, U.S. Environmental Protection Agency (E243-04), 4930 Page Rd., Durham, NC, 27703, USA Tel: +1 919 541 4802, Fax: +1 919 541 1379, E-mail: godowitch.james@epa.gov

Abstract

A diagnostic model evaluation effort has been performed to focus on photochemical ozone formation and the horizontal transport process since they strongly impact the temporal evolution and spatial distribution of ozone (O_3) within the lower troposphere. Results from the Community Multiscale Air Quality (CMAQ) modeling system are evaluated against surface and upper-air measurements from field studies during summer 2002 when several high O_3 episodes occurred in the eastern United States. Modeled O_3 and winds are compared to research aircraft measurements and wind profiler data, respectively, to investigate whether model underestimates of daily maximum 8-h ozone concentrations during high O_3 episodes might be attributable to discrepancies in either or both of these modeled processes. Comparisons of 10 AM surface O_3 concentrations, which are representative of O_3 levels in the residual layer aloft, revealed that model underestimation was greater at higher observed ozone levels. Mid-morning vertical ozone profiles corroborated this surface-level finding, as modeled concentrations tended to be lower than observed O_3 aloft. Net ozone production efficiency (OPE) results suggested photochemical ozone formation was comparable between the model and observations with composite OPE values of 6.7 and 7.6, respectively, within the afternoon planetary boundary layer. Evaluation of wind profiles revealed modeled wind speeds with the base four-dimensional data assimilation (FDDA) approach underestimated observed speeds by more than 2 m/s and direction was biased by about 20° in the nocturnal residual layer aloft as coarse resolution analysis fields involved in FDDA were found to inhibit modeled winds. These differences could produce large spatial displacements in modeled and observed ozone patterns within the region. Although sensitivity simulation results with the WRF meteorological model with FDDA using all available upper air profile observations displayed improvements in

capturing wind fields aloft, CMAQ maximum 8-h O₃ results using the improved wind fields also underestimated observations.

Key Words: diagnostic model evaluation, photochemical modeling, residual layer ozone, nocturnal low-level jet, four-dimensional data assimilation

1. Introduction

Three-dimensional (3-D) Eulerian photochemical models contain complex algorithms to simulate the relevant physical, chemical, and removal processes that govern the temporal evolution and spatial variability of ozone (O_3), other gaseous species, and aerosols. Further development and improvements of these modeling systems, however, is partly contingent upon feedback gained from model evaluation efforts, which gauge model performance based on comparisons of simulated results with observations.

Diagnostic model evaluation, one of four complimentary approaches encompassing a comprehensive model evaluation framework (Dennis et al., 2010), is designed to probe a particular modeled process in order to gain an understanding of the reasons for poor or good agreement between model results and observations. It is recognized that it is difficult to obtain absolute clarity when interpreting diagnostic evaluation results of an individual process due to the simultaneous interaction and non-linearity among the many processes governing the concentrations in a regional modeling system. Nevertheless, the motivation for this evaluation study was to gain insight into the potential cause(s) of the notable underestimation of modeled maximum O_3 values reported in operational evaluation studies (e.g. Mao et al., 2010; Appel et al., 2007, Godowitch et al., 2008a), which also contributed to the reduced modeled O_3 response relative to the observed change induced by emission changes and meteorological variability in recent dynamic model evaluation studies (Gilliland et al, 2008; Godowitch et al., 2010, Pierce et al., 2010).

Photochemical ozone production and horizontal transport, two key atmospheric processes that must be accurately simulated in order to reproduce O_3 formation and its spatial variability, respectively, are subjected to diagnostic evaluation. Modeled results of concentrations and winds are evaluated herein against available measurements with particular emphasis on conditions aloft. It is acknowledged that modeled O_3

concentrations are sensitive to the photochemical mechanism employed. Nevertheless, in this effort the Community Multi-scale Air Quality (CMAQ) model was applied with a single chemical mechanism (Carbon Bond-CB05). A detailed inter-comparison of 3 widely-used chemical mechanisms (CB4, CB05 and SAPRC99) already reported by Luecken et al. (2008) revealed SAPRC99 generated somewhat higher O₃ concentrations than CB05, and both simulated higher values than CB4.

Diagnostic chemical indicators analyzed herein require O₃ and certain precursor measurements that are not routinely available. Consequently, a 3-month period from summer 2002 was specifically selected to take advantage of both routine surface observations and also intensive field study measurements aloft via two instrumented research aircraft. In particular, nitrogen oxides (NO_x) and total nitrogen species (NO_y) concentrations were sampled along flight paths within the afternoon planetary boundary layer (PBL), enabling comparisons of ozone production efficiency and chemical age. As a prelude, evidence has indicated that a substantial portion of the O₃ existing aloft in the residual layer was actually formed much farther upwind during the previous day (Lin, 2008; Vukovich and Scarborough, 2005; Ryan et al., 1998). Consequently, modeled and observed O₃ concentrations from surface site measurements at 10 AM, representative of ozone entrained downward from the residual layer (Zhang and Rao, 1999), as well as from morning vertical profiles are investigated to determine if a model bias existed prior to the mid-day active photochemical ozone formation period.

It is essential that the diurnal evolution of the 3-D wind flow (speed and direction) field be accurately characterized by a dynamic meteorological model, which provides the winds and other parameter fields for photochemical model simulations. Wind field errors can lead to increasingly greater spatial displacements between modeled and observed spatial pollutant patterns contributing to modeled ozone errors. Although modeled and observed hourly wind profiles at radar profiler location were analyzed to investigate how

well the model reproduces the wind speed and direction over the entire day, more attention is focused on simulating the characteristics of the nocturnal low level jet (LLJ) during a representative multi-day high ozone episode, since the LLJ is an important horizontal transport mechanism of O₃ aloft and it generally develops near sunset and persists throughout the night in the mid-Atlantic region (Zhang et al., 2006).

A four-dimensional data assimilation (FDDA) approach using temporally varying 3-D objective analysis fields (Stauffer et al., 1991) was utilized in the base simulations of the MM5 meteorological model for our retrospective modeling application. Since more data aloft are now available to ingest into meteorological models equipped with FDDA than the temporally and spatially sparse routine upper air measurements used in earlier studies (Zhang et al., 2001, Rao et al., 2003), an evaluation of modeled wind fields subjected to FDDA against wind profiler observations that were not assimilated can provide valuable information about how well horizontal flow fields are simulated. Finally, sensitivity runs with options to the FDDA procedure and incorporating additional available observed upper air winds were undertaken with the Weather Research and Forecast (WRF) meteorological model to examine whether improvements in the strength and structure of the LLJ in the mid-Atlantic region could be achieved. The impact on O₃ using improved wind fields in a CMAQ simulation is also highlighted.

2. Model Description and Simulation Details

2.1 Chemical transport model

The CMAQ chemical transport model (v4.7) was applied in this study. The key components of the CMAQ model employed in this application were the Carbon Bond 05 (CB05; Luecken et al, 2008) chemical mechanism, asymmetric convective mixing scheme (ACM2) for vertical dispersion, and the piece-wise parabolic method (PPM) for the horizontal advection process (Byun and Schere, 2006).

The modeling domain encompassed the eastern two-thirds of the US and southeastern Canada with a 12-km grid cell size. There were 24 vertical model layers extending to a height of ≈ 15 km with 10 layers of varying thickness below 1 km, although the thicknesses of the first 3 layers were ≈ 40 m. Lateral boundary concentrations were prescribed by CMAQ results from a continental domain simulation with a 36-km grid cell size. Since the summer 2002 period was part of an annual simulation, initial conditions at the starting time (00 UTC) on June 1 were specified by the 3-D concentration field from the end of the previous day.

2.2 Meteorological modeling and data assimilation method

The meteorological fields provided for the CMAQ simulations were generated by the Penn State/NCAR fifth-generation mesoscale model (MM5 v3.7.4). The MM5 model was applied in a non-hydrostatic mode and the key physics modules used in this study included the Pleim-Xiu land surface scheme, Dudhia short-wave radiation and RRTM long-wave radiation models, Kain-Fritsch 2 cumulus and Reisner 2 microphysics parameterizations, and the same Asymmetric Convective Model (ACM2) for vertical mixing applied by CMAQ. In addition, a four-dimensional data assimilation (FDDA) approach, a widely-used technique applied in meteorological modeling of retrospective periods for air quality modeling efforts, involved nudging with 3-D objective analysis (OA) fields (Stauffer et al., 1991). The FDDA approach ensures that synoptic-scale forcing is accurately maintained during the course of the 5 consecutive simulation days during individual model runs. Otte (2008) reported more accurate meteorological parameters and better CMAQ performance results were obtained when the FDDA approach was applied in MM5 simulations than without it.

The FDDA procedure applied in MM5 for this study employed 3-hourly, 3-D OA fields of the horizontal wind components, temperature, and water vapor mixing ratio to nudge

the dynamically-generated model fields through an additional term containing weighting coefficients. The OA fields consisted of the gridded initialization analyses of National Weather Service Eta model, which was run 4 times daily as well as forecasted model output at 3 hours after initialization blended with available rawinsonde wind, temperature, and moisture measurements. The OA fields available for 2002 exhibited a 40 km horizontal grid resolution and only 5 vertical layers below 1 km. In the base case MM5 simulations, these OA fields were used to nudge the modeled parameter fields in layers above the PBL at all hours. In addition, 3-hourly 2-D OA surface wind fields were used to nudge model winds in the lowest layers of the PBL. Further details about the FDDA procedures and the reanalysis tools for regridding the OA fields are described in Gilliam and Pleim (2010). The input meteorological data sets for the CMAQ model runs were prepared by the Meteorology-Chemistry Interface Processor (MCIPv3.4) program, which extracts the 2-D and 3-D parameter fields needed by CMAQ and condenses the results from MM5's 34 vertical layer configuration, primarily in the upper layers, onto the 24 layer structure used by CMAQ.

The same FDDA approach has also been implemented in the Weather Research and Forecasting (WRF v3) meteorological model (Gilliam and Pleim, 2010), an updated successor of the MM5 model. Subsequent to the CMAQ runs for this study, the WRF model replaced MM5 as the meteorological driver for CMAQ. Consequently, results are reported from WRF sensitivity simulations using different FDDA options and additional observational wind data sets in an attempt to generate the most accurate modeled wind fields, especially to better characterize features of the nocturnal LLJ. Configured with the same physics modules, the WRF and MM5 models generate very similar wind fields (Figure A1, Supplemental Material).

2.3 Emissions modeling

Hourly gridded emissions were generated by the Sparse Matrix Operator Kernel Emissions (SMOKEv2.2) processing system. The anthropogenic emissions were obtained from the U.S. EPA's 2002 National Emissions Inventory, while major point source emissions were available from Continuous Emissions Monitoring System (CEMS) hourly measurements. The hourly gridded on-road vehicle emissions were generated by the MOBILE6.2 model for the entire modeling period. County-specific control program information from each state was also taken into account in the MOBILE6 modeling to provide better local estimates of mobile source emissions. Biogenic emissions of NO_x, isoprene, and other naturally-emitted VOC species were computed by the Biogenic Emissions Inventory System (BEISv3.14) model.

3. Measurement Systems and Data Analysis

3.1 Surface observations

Hourly O₃ observations were retrieved from the Air Quality System (AQS; <http://www.epa.gov/air/data/aqsdb.html>) and Clean Air Status and Trends Network (CASTNET; <http://www.epa.gov/castnet>) data bases. These measurements were spatially and temporally paired with CMAQ hourly average concentrations from the grid cells in which the sites were located. Although 63 rural-based CASTNET sites exist in the eastern US, concentrations from 34 monitoring sites located in the interior of the modeling domain and away from the domain boundaries were paired with modeled results in the same manner. Modeled and observed daily maximum 8-h average O₃

concentrations were determined from the hourly concentrations by computing running 8-h averages and then selecting the maximum value.

3.2 Aircraft measurements

The Department of Energy's Gulfstream (BNL-G1) research aircraft conducted sampling flights on selected afternoon periods (1600-2000 UTC) during July 2002. The long horizontal traverses at altitudes near the middle of the PBL extended over broad areas of southern New England and the northern part of the mid-Atlantic states (Kleinman et al., 2007). A spatial resolution of about 1 km was achieved with measurements processed at 10 s intervals. Numerous on-board instruments collected various gaseous species and aerosol parameters with detailed instrument descriptions given in Kleinman et al. (2007) and Springston et al. (2005). The relevant gas measurements included NO, NO₂, NO_y, and O₃. The secondary nitrogen species group (NO_z) was determined by subtracting NO_x (i.e. NO+NO₂) from the total nitrogen (NO_y) concentration. These data were paired with modeled values from the appropriate grid cell aloft and temporally-interpolated to the time of the measurements. Owing to the much finer resolution of the measurements, all observations within the same CMAQ grid cell were averaged and matched up with the modeled grid concentrations.

The University of Maryland (UM) research aircraft obtained measurements in the mid-Atlantic states during June and July 2002 and in northern New England states on selected days through mid-August. The sampling flights consisted primarily of ascent/descent spirals near small airport locations (Hains et al., 2008) to obtain vertical profiles of O₃, SO₂, CO, air temperature, and relative humidity from near the surface to nearly 3 km above ground level (AGL). A complete description of the UM aircraft instrument package and the data processing was discussed by Taubman et al. (2004). The latitude/longitude position of each airport was used to determine the particular

model vertical column to match up with the observed profile. Observations within each CMAQ layer were averaged and paired with the model's layer-average concentrations, which were also temporally interpolated to the time of the spiral.

During aircraft flights in the summer 2002, mid-morning pollutant profiles were obtained at upwind locations from the mid-Atlantic urban areas (e.g., Washington, DC , Richmond, VA). A morning flight was often followed by an afternoon flight consisting of spirals at selected small airport locations near to or downwind of these major urban areas. The flights in northern New England during August differed in the sense that they were made at locations a considerable distance downwind from any major urban area or source region so the concentrations were more likely subjected to long-range transport.

3.3 Upper air wind measurements

Wind profilers from the Cooperative Agency Profiler (CAP) network consist of small UHF Doppler radar systems operated continuously at a 915 MHz frequency by various environmental agencies in certain eastern states. During summer 2002, wind profiler sites existed in the mid-Atlantic region and in New England states (<http://madis-data.noaa.gov/cap>). Wind speed and direction were sampled for 55 minutes of each hour and the time stamp is set at the start hour of the data. Wind speed and direction accuracies are prescribed to be ± 1 m/s and $\pm 10^\circ$, respectively. The minimum height of a valid wind measurement differed somewhat among these sites with the first level at near 124 m AGL, which was still sufficiently low to capture the LLJ wind maxima during nocturnal hours. The vertical resolution of the measurements is 55 m at the shorter range gate and winds were generally obtained to about 2 km AGL where the signal began to deteriorate. The observed winds were interpolated to the mid-layer height of each model layer to expedite comparisons with the modeled wind speeds and directions.

Additionally, the modeled wind directions were also adjusted from the Lambert conformal projection onto the latitude/longitude coordinates of each profiler site.

4. Results

4.1 Analyses of concentrations and diagnostic chemical indicators

The day-to-day variability in the modeled and observed daily maximum 8-h O₃ concentrations over the 3-month period is displayed in Figure 1 by the mean and 95th percentile values. These results were determined from modeled values and CASTNET site observations in the eastern US. Several prominent multi-day high O₃ episodes are exemplified by those days when the observed daily maximum 8-h O₃ at the 95th percentile level exceeded 90 ppb. The gradual rise of maximum O₃ concentrations and eventual decrease in ozone levels is associated with the large-scale synoptic forcing associated with the movement of air masses and frontal passages across the region. This ozone variation on the synoptic scale cycle is replicated very well by the model based on the close matching of the day-to-day variability between these modeled and observations. These results are also supportive of the findings from the scale analysis of observed and modeled O₃ time series spanning extended periods, which revealed the model closely captured the ozone variability on the synoptic time scale (Hogrefe et al., 2004). However, the modeled results clearly underestimated maximum O₃ levels on several high ozone days in Figure 1, especially at the 95th percentile. In particular, the observed and modeled mean daily maximum 8-h O₃ values at the 95th percentile from the 24 high ozone days were 96 ppb and 84 ppb, respectively, which compares to corresponding values from non-episode days of 75 and 70 ppb, respectively. Since the modeled results exhibited a much greater negative bias on the highest O₃ cases, additional analyses were pursued with the observed and modeled O₃ data from selected episode days; namely, June 10-11, June 20-25, July 1-2, July 8-9, July 15-18, August 1-

2, and August 11-15. Evaluation of winds within the lower troposphere below ≈ 2 km focused on the August 11-15 period. The synoptic conditions on all these cases displayed a broad high pressure area in the mid-Atlantic and southeastern states with a southwesterly flow extending from the Ohio River Valley region into the northeastern US, which Hegarty et al. (2007) noted as the primary pattern associated with high O_3 over the model domain during the summer 2002.

It is worthwhile to briefly examine the chemical and transport processes involved in the build-up of concentrations during a high ozone episode event. Based on model results, Figure 2 illustrates the gradual rise of simulated O_3 over a multi-day period along a trajectory path backward in space and time from a downwind starting location where high ozone existed (Figure 2a). The paths of back-trajectories released at 500 and 1000 m from the location of ozone profiles near Albany, NY were generated by the HYSPLIT trajectory model (http://www.arl.noaa.gov/HYSPLIT_info.php) using modeled base case wind fields. The trajectories were initiated at the time of the observed profile (17 UTC on August 12) and spans an 80 hour period backward in time (Figure 2b). Figure 2c depicts the modeled O_3 concentrations along the back-trajectory path at 500 m AGL and in layer 1 below this elevated trajectory position. Concentrations aloft in Figure 2c steadily evolved from < 40 ppb at 1100 km upwind and 80 hours earlier up to 85 ppb at the time and place of the ozone profiles in Figure 2a. In contrast to the dramatic swings displayed in layer 1 O_3 concentrations from each night to day, O_3 aloft was maintained at about the same concentrations along the trajectory path within the nocturnal residual layer. These results also reveal that as the morning vertical mixing process proceeds, surface ozone levels rise toward values existing aloft and then photochemical production provides an additional contribution to higher O_3 levels within the PBL during successive daytime periods. This example case, showing lower modeled O_3 than observed concentrations over the entire PBL by about 15 ppb (Figure 3a), provides an incentive to

ascertain whether the chemical and/or transport processes might be attributable to the model's underestimation of O₃ during episodic conditions.

Analyses were undertaken to determine how modeled O₃ concentrations compared to surface observations at 10 AM during the ozone episode cases and aloft. As noted earlier, surface O₃ concentrations at this time are a strong indicator of concentrations existing in the residual layer since downward mixing occurring during the erosion of the nocturnal inversion layer entrains O₃ from aloft (Zhang and Rao, 1999). The results in Figure 3a indicate modeled O₃ at 10 AM exhibited an increasingly larger underestimation at the higher observed concentration levels, which reveals modeled values are already low relative to observed values prior to the active photochemical formation period. Results of hourly rates of change of surface O₃ (Figure A2, Supplemental Material) also provide evidence that less overall O₃ in the model is entrained downward as the PBL grows during the morning period. Interestingly, the surface results in Figure 3a are somewhat similar to the results obtained aloft (Figure 3b). Results in Figure 3b represent modeled and observed O₃ concentrations determined over the residual layer, specified to be between 500 and 1500 m AGL, from all mid-morning profiles. These results also indicate modeled O₃ aloft to be generally lower than observed O₃ concentrations, especially above 60 ppb. Another interesting feature is evident in Figure 3b at lower O₃ concentration levels where modeled values sometimes exceeded the observations aloft, which may be evidence of possible spatial displacements in the modeled ozone pattern to be explored later.

Figure 4 depicts the mean modeled and observed O₃ derived from all morning profiles, which also reinforces the results at the surface. These O₃ profiles were computed from aircraft spiral measurements and corresponding model results between 0800 and 1000 AM. Figure 4a indicates modeled O₃ values were indeed lower across a large portion of the residual layer from about 400 m to 1500 m AGL at mid-Atlantic sites.

The reason that modeled values were greater than observed ozone concentrations closer to the surface is believed to be due to higher modeled PBL heights (Z_i) (i.e. mean modeled and observed Z_i were 534 m and 264 m, respectively, from all profiles), which suggests vertical mixing had already entrained the O_3 from aloft sooner in the model than in the observations. Figure 4b displays a significant model ozone underprediction at northern New England sites during a high ozone episode day (i.e., August 13, 2002) with observed O_3 in the residual layer exceeding 90 ppb compared to modeled values under 70 ppb. These extremely high observed values at the New Hampshire / Vermont sites are likely due to long-range transport rather than to local chemical production since this area is a considerable distance from major ozone precursor emission source regions (Griffin and Talbot, 2004).

Figure 5 presents the modeled and observed mean ozone profiles based on all mid-afternoon profiles. To better assess the vertical structure of O_3 within the PBL, height has been normalized by the simulated and observed PBL heights due to spatial and daily PBL differences. These mean modeled and observed profiles reveal the characteristic decrease in O_3 above the PBL with mean values in both modeled and observed results approaching 65 ppb. The mean observed profile indicates that O_3 gradually increases within the PBL with observed values greater than model values by about 5-8 ppb, however, at $+1\sigma$ (σ = standard deviation SD) above the means the observed values exceeded modeled results by nearly 10 ppb. In contrast, the modeled O_3 profile is generally more uniform with a gradual decrease in the upper portion of the PBL. The lower part of the observed profiles may be impacted by an O_3 titration effect from surface emissions in the vicinity of the airport sites, which are near urban areas since observed CO concentrations in profiles (not shown) were found to be nearly double the modeled values. Due to the model's horizontal grid cell size, this feature could not be resolved.

Diagnostic evaluation of the photochemical ozone formation process was performed with concentrations aloft. Modeled and observed concentrations of NO_z ($\text{NO}_z = \text{NO}_y - \text{NO}_x$) and NO_y aloft were analyzed from the horizontal traverses within the mid-afternoon PBL during July 2002. The analysis approach of Olszyna et al. (1998) involved sorting NO_y concentrations into bins with each bin containing 5% of the values within the concentration distribution. Results of a linear regression fit to the modeled and observed average binned concentrations revealed slopes of 0.86 and 0.89, respectively, indicating the modeled chemical age as represented by the $\text{NO}_z / \text{NO}_y$ ratio is of comparable maturity with the observed air mass in the region.

A valuable diagnostic chemical probe (Arnold et al., 2003) involves analysis of the O_3 to NO_z relationship for both sets of modeled and observed concentrations aloft. The slope fitted to these species is considered an indicator of net ozone production efficiency (OPE) since it represents an estimate of the net ozone production from each emitted NO_x molecule that is oxidized to NO_z . However, the net OPE estimate must be considered an upper limit since the difference in the deposition loss over time between O_3 and various species included in NO_z is unaccounted for in deriving this OPE value. Nevertheless, after applying the same approach noted above, Figure 6 displays the best-fit linear regression slope to the modeled and observed O_3 and NO_z values derived from all cases. The composite slopes derived from all modeled and observed data are quite comparable with net OPE values of 6.7 and 7.6, respectively. However, net OPE differed on individual cases with observed (modeled) values of 7.1 (6.5), 6.2 (6.0), 3.5 (4.3), 8.1 (6.4), 7.4 (7.2), 6.6 (4.9), and 6.4 (5.4) on July 12, 13, 14, 16, 17, 21 and 22, respectively. Variations in these OPE values is to be expected due to differences in various factors influencing photochemical production (e.g., incoming solar radiation, temperatures) among these cases. The modeled net OPE values also correlated with observed values although they are generally slightly lower. These net OPE values aloft

are quite comparable to results derived from various surface monitoring sites in the region (Godowitch et al., 2008b). In particular, a net OPE of 7.0 for summer 2002 was found at the Pinnacle State Park surface monitoring site in western New York state, a location passed over during several aircraft flights. Griffin et al. (2004) determined a net OPE of 9.1 from summer 2002 data at a surface monitoring site in New Hampshire, however, an adjusted net OPE of 7.7 was determined after accounting for dry deposition.

4.2 Horizontal transport analyses

A diagnostic evaluation of modeled wind profiles was possible with an independent data set of wind profiler measurements that were not incorporated in the OA fields used in FDDA for the MM5 model's base simulations. In an initial comparison of winds aloft, differences in wind speeds (modeled - observed) were determined from hourly modeled and observed profiles over the 3-month period from all profiler sites. Results displayed in the vertical time section in Figure 7 reveal a noticeable model speed bias of close to -1.6 m/s during the nocturnal hours at low altitudes where the LLJ is generally found. During daytime hours, relatively small differences exist and are within the accuracy of the profiler measurements. A similar feature was also apparent in model comparisons against nocturnal wind speeds from profiler sites in the central US where the Great Plains nocturnal LLJ occurs (Gilliam and Pleim, 2010).

Figure 8 displays modeled and observed wind speed and direction profiles averaged over the nocturnal hours (2000 to 0600 local time) from the August episode period (August 11-14). This period was selected for more detailed analyses to provide a better description of the transport differences between the model and observations under typical elevated ozone conditions. Modeled wind speeds in Figure 8a are indeed slower by more than 2 m/s over a substantial portion of the residual layer. Furthermore,

modeled mean wind directions aloft in Figure 8b displayed a more southerly bias of at least 20°. These base case results were not unique to this profiler site, since comparable results were also found at the other mid-Atlantic sites. At sites along the entire eastern seaboard, modeled wind speeds aloft were found to be less than to observed values, as demonstrated in Figure A3 of Supplemental Material.

The impact of the modeled and observed wind differences on horizontal transport of pollutants was further explored using HYSPLIT trajectory analysis. Hourly mean wind profiles were computed with the model results and observations at selected sites from the multi-day August episode. The hourly mean modeled and observed wind profiles were used in the same manner applied by Gilliam et al. (2006) as the time-varying, 3-D wind fields. In our analysis, a trajectory release height of 500 m AGL was prescribed with a release time of 00 UTC (2000 local time). The separation distance between the modeled and observed trajectory positions was computed as well as the total downwind distance traveled by the modeled and observed trajectories. Figure 9a reveals a steadily growing spatial separation between the modeled and observed trajectory positions that reached about 150 km after 10 hours of nighttime travel from each site in the mid-Atlantic region. Most of the displacement is attributed to the wind speed differences, however, the modeled wind direction bias also contributed to the growing separation distance during the night. Thus, the variation in the modeled and observed trajectory paths indicates that large spatial displacements developed overnight between modeled and observed pollutant fields aloft. During the daytime hours (i.e., after 12 hours), the separation distance does not change appreciably indicating better agreement between the daytime modeled and observed winds. The notable results in Figure 9b show that observed travel distances are indeed greater than modeled results by about 100 km or more after 10 hours due primarily to the slower modeled nocturnal wind speeds and these differences in travel distance prevailed during the duration of the 24-h period.

These results reveal that modeled horizontal transport was indeed underestimated along the mid-Atlantic region during nocturnal periods with strong nocturnal jets. Evidence of spatial ozone displacements by the model are exhibited in Supplemental Material (Figures A4, A5).

Sensitivity runs with the WRF model were undertaken using different FDDA options as well as additional upper air data sets to assess the effects on wind fields and the nocturnal LLJ during the key August 11-14 episode. Table A1 in Supplemental Material documents the peak speeds and related characteristics of the nocturnal LLJ indicating the underestimation by the modeled base case results. From a particular sensitivity run, Figure 10a,b illustrate the modeled wind flow patterns at ≈ 400 m AGL (layer 7) on August 11 at 0800 UTC for the base case with FDDA and no FDDA below 2 km simulations, respectively. A nocturnal jet with higher wind speeds is apparent in the mid-Atlantic region with a south-southwesterly flow, however, the results in Figure 10b with no FDDA below 2 km (i.e. below layer 17) exhibit stronger wind speeds in the mid-Atlantic jet as well as in other areas of the model domain. These dramatic wind field differences between the base and no FDDA below 2 km cases demonstrates the negative effect of applying FDDA in the lowest layers (i.e. when PBL heights at night are <100 m) using the rather coarse vertical resolution of the 3-D OA fields, which could not adequately resolve the nocturnal LLJ. Clearly, the dynamically-generated fields of the numerical model were inhibited from fully developing a nocturnal jet in the mid-Atlantic region since the base FDDA procedure applied weighting to all layers above the shallow nocturnal PBL height.

The modeled wind speed profiles in Figure 11, averaged over the nocturnal period from selected sensitivity runs, reveal that increasingly better agreement with the observed profile occurred as the FDDA weighting coefficient was reduced. The sensitivity run denoted by profile-assim (SENS9), which involved modification of the

original OA fields by the inclusion of all wind profiler data and VAD (Velocity Azimuth Display) Doppler radar wind measurements (Michelson and Seaman, 2000) along with no surface FDDA, generated modeled results that were closest to observed winds aloft. However, the observed average LLJ speed was slightly overestimated and the modeled LLJ height was slightly lower than the observed jet height. Additional results in Figures A6, A7 of Supplemental Material show how well the winds aloft are captured over the diurnal period from various sensitivity runs.

CMAQ was applied with the meteorological fields from the SENS9 run to examine the impact on maximum ozone fields and maximum 8-h O₃ levels relative to the base case for the August episode. Results for maximum 8-h O₃ revealed a mean bias of -10.1 and -14.5 ppb, and mean error of 12.7 and 16.3 ppb from the base case and SENS9 runs, respectively, from 397 AQS rural sites. While the SENS9 results contained improved wind flow fields, horizontal transport was greater which also caused maximum 8-h O₃ levels to be slightly lower than in the base case as evident in the mean bias values. Maximum 8-h O₃ levels from the SENS9 results also exhibited underestimates just as in the base case (Figure 12a). However, Figure 12b reveals that notable differences in maximum O₃ also existed between these simulation results in various areas due to the horizontal transport differences. In particular, an interesting outcome is demonstrated in Figure 13 by the O₃ concentrations along trajectories originating from the same urban source locations and for the same release time (11 UTC). Although similar O₃ concentrations were generated by both simulations, the trajectories based on these two different wind fields followed different paths, as anticipated, that impact different locations downwind after 2 travel days. The stronger and more westerly component in the SENS9 wind flows caused trajectory paths that were longer and generally to the right of those in the base case. On the other hand, a trajectory emanating from a Maryland location in Figure 13b with the stronger nocturnal SENS9 winds reached southern CT,

while the base case counterpart in Figure 13a only crossed southern Long Island. Unfortunately, evaluation results with surface observational site values in CT were inconclusive regarding which model run provided better performance.

5. Summary

A diagnostic evaluation effort has examined OPE, an indicator of O₃ production and the horizontal transport process in the CMAQ modeling system to take advantage of field study measurements aloft under primarily high O₃ conditions during summer 2002. Although modeled surface 10 AM O₃ and morning residual layer O₃ concentrations were generally found to be biased low at the higher observed concentration levels, modeled net OPE values were quite comparable to observed results in the mid-afternoon PBL. Evaluation of modeled base case wind profiles against an independent set of wind profiler measurements revealed that nocturnal wind speeds were underestimated in the low level jet and residual layer, and modeled wind directions exhibited a slight southerly bias in the mid-Atlantic region. Variations in trajectory paths due to observed and modeled wind flow differences help explain the reason that large spatial displacements of pollutant patterns can grow over the course of the nocturnal period. Sensitivity simulations with the WRF meteorological model showed improvements in capturing nocturnal transport aloft when additional available wind profile data were incorporated into the FDDA approach and surface nudging was omitted. These results demonstrate the importance of accurately simulating flow fields aloft, particularly at night, since overnight transport of O₃ and its precursors trapped aloft in the nighttime residual layer are subsequently entrained to the surface in downwind areas far from emission sources. While a CMAQ simulation utilizing improved wind fields underestimated maximum O₃ levels just as in the base case, a better FDDA approach utilizing more available upper air data sets was identified to more accurately replicate pollutant transport, which allows

a forthcoming diagnostic evaluation to focus on other key input factors and model processes.

Acknowledgements

Thanks are extended to Stephen Springston (Brookhaven National Laboratory) and to Russell Dickerson (University of Maryland) for making available their aircraft data sets. NOAA / ESRL / GSD is recognized for maintenance and access to the MADIS archive of CAP wind profiler measurements. The VAD data are from the Research Data Archive (RDA) is maintained by the Computational and Information Systems Laboratory (CISL) at the National Center for Atmospheric Research (NCAR). NCAR is sponsored by the National Science Foundation (NSF). The original data are available from the RDA (<http://dss.ucar.edu>) in dataset number ds337.0. The U.S. Environmental Protection Agency through its Office of Research and Development funded and managed the research described herein. Although it has been subjected to Agency review and approved for publication.

References

- Appel, K.W., Gilliland, A.B., Sarwar, G., Gilliam, R.C., 2007. Evaluation of the Community Multiscale Air Quality (CMAQ) model version 4.5: Sensitivities impacting model performance; part I – ozone. *Atmospheric Environment*, 41, 9603-9615.
- Appel, K.W., Roselle, S.J., Gilliam, R.C., Pleim, J.E., 2010. Sensitivity of the Community Multiscale Air Quality (CMAQ) Model v4.7 results for the eastern United States to MM5 and WRF meteorological drivers. *Geoscientific Model Development*, 3, 169-188.
- Arnold, J.R., Dennis, R.L., Tonnesen, G.S., 2003. Diagnostic evaluation of numerical air quality models with specialized ambient observations: testing the Community Multiscale Air Quality modeling system (CMAQ) at selected SOS 95 ground sites.

- Atmospheric Environment, 37, 1185-1198, doi:10.1016/S1352-2310(02)01008-7
- Byun, D., Schere, K.L., 2006. Review of the governing equations, computational algorithms, and other components of the Models-3 Community Multiscale Air Quality (CMAQ) modeling system. *Applied Mechanics Reviews*, 59, 51-77.
- Dennis, R.L., Fox, T., Fuentes, Gilliland, A., Hanna, S., Hogrefe, C., Irwin, J., Rao, S.T., Scheffe, R., Schere, K., Steyn, D., Venkatram, A., 2010. A framework for evaluating regional-scale numerical photochemical modeling systems. *Environmental Fluid Mechanics*, doi10.1007/s10652-009-9163-2
- Gilliam, R.C., Pleim, J.E., 2010. Performance assessment of new land surface and planetary boundary layer physics in the WRF ARW. *Journal of Applied Meteorology and Climatology*, 49, 760-774.
- Gilliam, R.C., Hogrefe, C., Rao, S.T., 2006. New methods for evaluating meteorological Models used in air quality applications. *Atmospheric Environment*, 40, 5073-5086, doi:10.1016/j.atmosenv.2006.01.023.
- Gilliland, A.B., Hogrefe, C., Pinder, R.W., Godowitch, J.M., Foley K.L., Rao, S.T., 2008. Dynamic evaluations of regional air quality models: Assessing changes in O₃ stemming from changes in emissions and meteorology. *Atmospheric Environment*, 42, 5110-5123.
- Godowitch, J.M., Gilliland, A.B., Draxler, R.R., Rao, S.T., 2008a. Modeling assessment of point source NO_x emission reductions on ozone air quality in the eastern United States. *Atmospheric Environment*, 42, 87-100.
- Godowitch, J.M., Hogrefe, C., Rao, S.T., 2008b. Diagnostic analyses of a regional air quality model: Changes in modeled processes affecting ozone and chemical-transport indicators from NO_x point source emission reductions. *Journal of Geophysical Research*, doi:10.1029/2007JD009537.
- Godowitch, J.M., Pouliot, G.A., Rao, S.T., 2010. Assessing multi-year changes in

- modeled and observed urban NOX concentrations from a dynamic model evaluation perspective. *Atmospheric Environment*, 44, 2894-2901, doi:10.1016/j.atmosenv.2010.04.040
- Griffin, R.J., Johnson, C.A., Talbot, R.W., Mao, H., Russo, R.S., Zhou, Y., Sive, B.C., 2004. Quantification of ozone formation metrics at Thompson Farm during the New England Air Quality Study (NEAQS) 2002. *Journal of Geophysical Research*, 109, D24302, doi:10.1029/2004JD005344
- Hains, J.C., Taubman, B.F., Thompson, A.M., Stehr, J.W., Marufu, L.T., Doddridge, B.G., Dickerson, R.R., 2008. Origins of chemical pollution derived from mid-Atlantic aircraft profiles using a clustering technique. *Atmospheric Environment*, 42, 1727-1741, doi:10.1016/j.atmosenv.2007.11.052
- Hegarty, J., Mao, H., Talbot., 2007. Synoptic controls on summertime surface ozone in the northeastern United States. *Journal of Geophysical Research*, 112, D14306, doi:10.1029/2006JD008170
- Hogrefe, C., Biswas, J., Lynn, B., Civerolo, K., Ku, J.Y., Rosenthal, J., Rosenweig, C., Goldberg, R., Kinney, P.L., 2004. Simulating regional-scale ozone climatology over the eastern United States: model evaluation results. *Atmospheric Environment*, 38, 2627-2638, doi:10.1016/j.atmosenv.2004.02.033
- Kleinman, L.I., Daum, P.H., Lee, Y.N., Senum, G.I., Springston, S.R., Wany, J., Berkowitz, C., Hubbe, J., Zaveri, R.A., Brechtel, F.J., Jayne, J., Onasch, T.B., Worsnop, D., 2007. Aircraft observations of aerosol composition and ageing in New England and mid-Atlantic states during the summer 2002 New England Air Quality Study field campaign. *Journal of Geophysical Research*, 112, D09310, doi:10.1029/2006JD007786
- Lin, C., 2008. Impact of downward mixing ozone on surface ozone accumulation in southern Taiwan. *Journal of Air and Waste Management Association*, 58:562-579,

doi:10.3155/1047-3289.58.4.562

- Luecken, D.J., Phillips, S., Sarwar, G., Jang, C., 2008. Effects of using the CB05 vs SAPRC99 vs CB4 chemical mechanism on model predictions: Ozone and gas-phase photochemical precursor concentrations. *Atmospheric Environment*, 42, 5805-5820, doi:10.1016/j.atmosenv.2007.08.056
- Mao, H., Chen, M., Hegarty, J.D., Talbot, R.W., Koermer, J.P., Thompson, A.M., Avery, M.A., 2010. A comprehensive evaluation of seasonal simulations of ozone in the northeastern US during summers 2001-2005. *Atmospheric Chemistry and Physics*, 10, 9-27.
- Michelson, S.A., and Seaman, N. L., 2000. Assimilation of NEXRAD-VAD winds in summertime meteorological simulations over the northeastern United States. *J. Appl. Meteor.*, 39, 367-383.
- Olszyna, K.F., Bailey, E.M., Simonaitis, R., Meagher, J.F., 1998. O₃ and NO_y relationships at a rural site. *Journal of Geophysical Research*, 77, D7, 14557-14563, doi:10.1029/94JD00739
- Otte, T., 2008: The impact of nudging in the meteorological model for retrospective air quality simulations. Part I: Evaluation against National Observation Networks. *Journal of Applied Meteorology and Climatology*, 47, 1853-1867, doi:10.1175/2007JAMC1790.1
- Pierce, T., Hogrefe, C., Rao, S.T., Porter, P.S., Ku, J., 2010. Dynamic evaluation of a regional air quality model: Assessing the emissions-induced weekly ozone cycle, *Atmospheric Environment*, 44, 3583-3596, doi: 10.1016/j.atmosenv.2010.05.046
- Ryan, W.F, Doddridge, Dickerson, R.R., Morales, R.M., Hallock, K.A., Roberts, P.T., Blumenthal, D.L., Anderson, J.A., Civerolo, K.L., 1998. Pollutant transport during a regional O₃ episode in the mid-Atlantic states. *Journal of Air and Waste Management Association*, 48:786-797.

- Springston, S.R., Kleinman, L.I., Brechtel, F., Lee, Y.-N., Nunnermacker, L.J., Wang, J., 2005. Chemical evolution of an isolated power plant plume during the TexAQS 2000 study, *Atmospheric Environment*, 39, 3431-3443.
- Stauffer, D.R., Seaman, N.L., Binkowski, F.S., 1991: Use of four-dimensional data assimilation in a limited area mesoscale model. Part II: Effects of data assimilation within the planetary boundary layer. *Monthly Weather Review*, 119, 734-754.
- Taubman, B.F., Hains, J.C., Thompson, A.M., Marufu, L.T., Doddridge, B.G., Stehr, J.W., Piety, C.A., Dickerson, R.R., 2006. Aircraft vertical profiles of trace gas and aerosol pollution over the mid-Atlantic United States: Statistics and meteorological cluster analysis. *Journal of Geophysical Research*, 111, D10S07, doi:10.1029/2005JD006196
- Taubman, B.F., Marufu, L.T., Piety, C.A., Doddridge, B.G., Stehr, J.W., Dickerson, R.R., 2004. Airborne characterization of the chemical, optical and meteorological properties and origins of a combined ozone-haze episode in the eastern United States. *Journal of Atmospheric Sciences*, 61, 1781-1793.
- Vukovich, F.M., Scarborough, J., 2005. Aspects of ozone transport, mixing, and chemistry in the greater Maryland area. *Atmospheric Environment*, 39, 7008-7019, doi:10.1016/j.atmosenv.2005.07.054
- Yu, S., Mathur, R., Kang, D., Schere, K., Eder B., Pleim, J., 2006. Performance and diagnostic evaluation of ozone predictions by the Eta-Community Multiscale Air Quality forecast system during the 2002 New England Air Quality Study. *Journal of Air and Waste Management Association*, 56:1459-1471.
- Zhang, D., Zhang, S., Weaver, S.J., 2006. Low-level jets over the mid-Atlantic states: Warm season climatology and a case study. *Journal of Applied Meteorology and Climatology*, 45, 194-209.
- Zhang, J., Rao, S.T., 1999. The role of vertical mixing in the temporal evolution of

ground-level ozone concentrations. *Journal of Applied Meteorology*, 38, 1674-1691.

Zhang, K., Mao, H., Civerolo, K., Berman, S., Ku, J.Y., Rao, S.T., Doddridge, B., Philbrick, C.R., Clark, R., 2001. Numerical investigation of boundary layer evolution and nocturnal low-level jets: local versus non-local PBL schemes. *Environmental Fluid Mechanics*, 1, 171-208.

List of Figures

- Figure 1. Modeled and observed mean and 95th percentile values of daily maximum 8-hour ozone concentrations determined from results at rural CASTNET site locations in the eastern US during the 92 day period from June 1 through August 31, 2002.
- Figure 2. a) Modeled and observed UM aircraft ozone profiles at S. Albany, NY near 17 UTC on August 12, 2002, b) paths of backtrajectories released at 500 m and 1000 m AGL at the same time as the profiles in a) and traveling 80 hours backward in time, c) modeled hourly ozone concentrations at backtrajectory positions at 500 m and below in layer 1. Vertical dashed lines in c) designate the time of sunrise on each day of this travel period.
- Figure 3. a) Modeled ozone concentrations at 10 AM (local time) versus observed 10 AM ozone levels from rural eastern surface AQS sites during summer 2002 ozone episode days and b) modeled residual layer ozone versus observed residual layer ozone levels from UM aircraft profiles obtained during summer 2002 experimental days. The box/whisker results depict values at the median (line inside the boxes), box edges denote the 25th and 75th percentiles and whiskers extend to the 10th and 90th percentiles.
- Figure 4. Mid-morning average modeled and observed UM aircraft ozone profiles a) from all sites in the mid-Atlantic region during June/July 2002 experimental cases and b) from 3 sites in VT/NH during August 13, 2002. The dashed lines represent ± 1 standard deviation (SD) from the average values.
- Figure 5. Modeled and UM aircraft average ozone profiles from mid-Atlantic and New England locations from mid-afternoon periods during summer 2002 episode cases. Height (z) is

normalized by the PBL height (Z_i). Dashed lines represent concentrations at ± 1 standard deviation (SD) from average values.

- Figure 6. Relationship between ozone and NO_z from model results and BNL aircraft measurements along horizontal traverses near the middle of the PBL in the mid-afternoon during summer 2002 field study days. Lines depict the slopes from linear regression fits to the modeled and observed results. Each symbol represents a value derived over 5% increments of the observed and modeled concentration distributions.
- Figure 7. Vertical time section of the average wind speed difference (modeled – observed) over the diurnal cycle based on modeled and observed profiles from all eastern radar wind profiler sites during the summer 2002 period. Isopleths are given in units of m/s.
- Figure 8. Modeled (gray) and observed (rose) a) wind speed and b) direction profiles averaged over the nocturnal periods of August 11-15, 2002 at Ft. Meade, MD. Boxes span the 25th to 75th percentiles, and whiskers in a) extend from 10th to 90th percentiles.
- Figure 9. a) Spatial separation between modeled (with base FDDA) and observed forward trajectory positions with time and b) total travel distance of the trajectories based on hourly modeled and observed winds averaged over the August 2002 episode days. A starting time of 00 UTC and a release height of 500 m AGL were used for each trajectory from FME (Ft. Meade, MD), RUT (New Brunswick, NJ), and RCH (Richmond, VA). The RUT trajectory is abbreviated because it reached the eastern model boundary.
- Figure 10. Wind flows depicting speeds (color tiles) and directions (arrows) near 500 m AGL at 0800 UTC on August 11, 2002 from WRF simulations. a) base FDDA and b) no FDDA below 2 km AGL.
- Figure 11. Modeled results averaged over the nocturnal period from different WRF simulations using different FDDA options versus an observed nocturnal average wind speed profile at Ft. Meade, MD from August 11, 2002. The observed profile has been truncated near 1000 m since profile data above this level were not available during all hours.
- Figure 12. a) Modeled maximum 8-h O_3 field using improved wind fields (SENS9) on August 12, 2002 and AQS site values (circles), and b) differences in maximum 8-h O_3 (SENS9 – base) results.
- Figure 13. Ozone from CMAQ runs is depicted along the paths of forward trajectories released at 500 m AGL on August 11, 2002 starting at 1100 UTC and traveling 50 hours downwind of selected locations using a) base case and b) SENS9 sensitivity run wind fields.

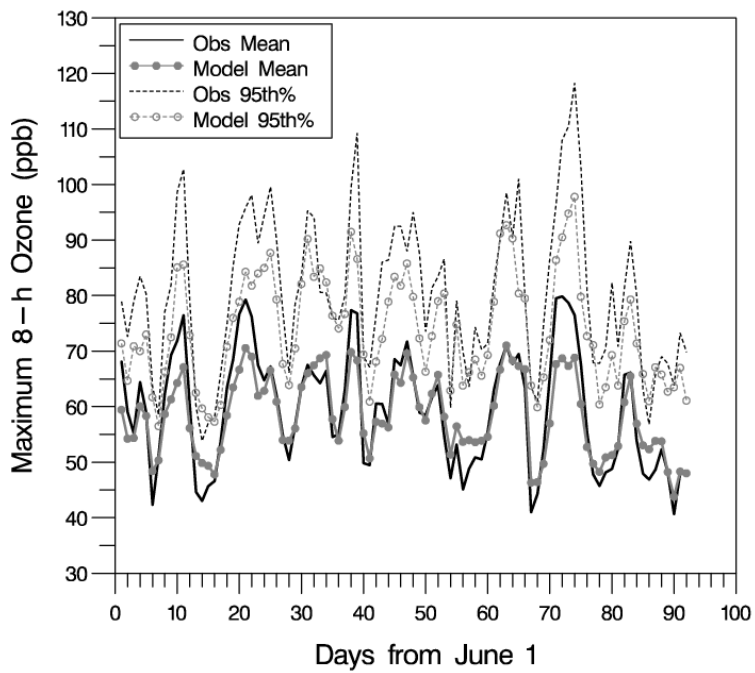


Figure 1. Modeled and observed mean and 95th percentile values of daily maximum 8-hour ozone concentrations determined from results at rural CASTNET site locations in the eastern US over the 92 day period from June 1 through August 31, 2002.

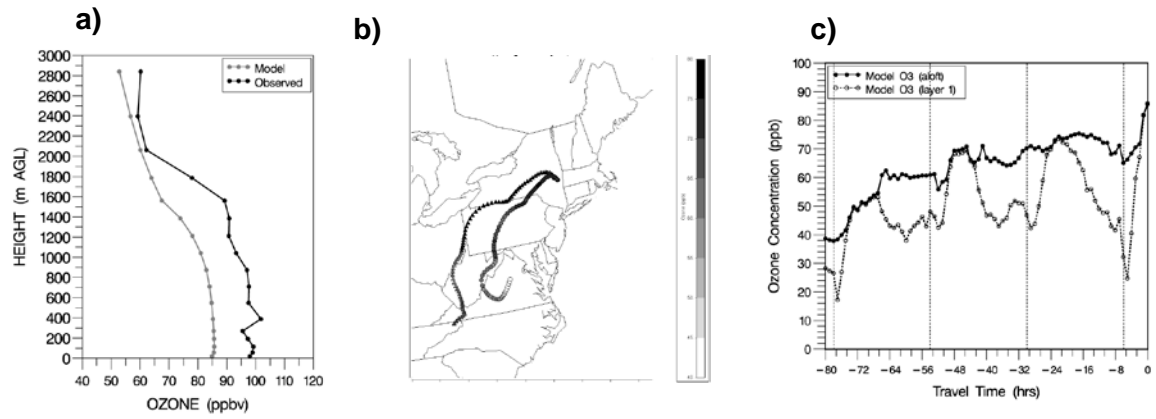


Figure 2. a) Modeled and observed UM aircraft ozone profiles near S. Albany, NY at 17 UTC on August 12, 2002, b) paths of backward trajectories released at 500 m and 1000 m AGL at the same time as the profiles in a) and traveling 80 hours backward in time, c) modeled hourly ozone concentrations at backward trajectory positions at 500 m and below in layer 1. Vertical dashed lines in c) designate the time of sunrise on each day of this travel period.

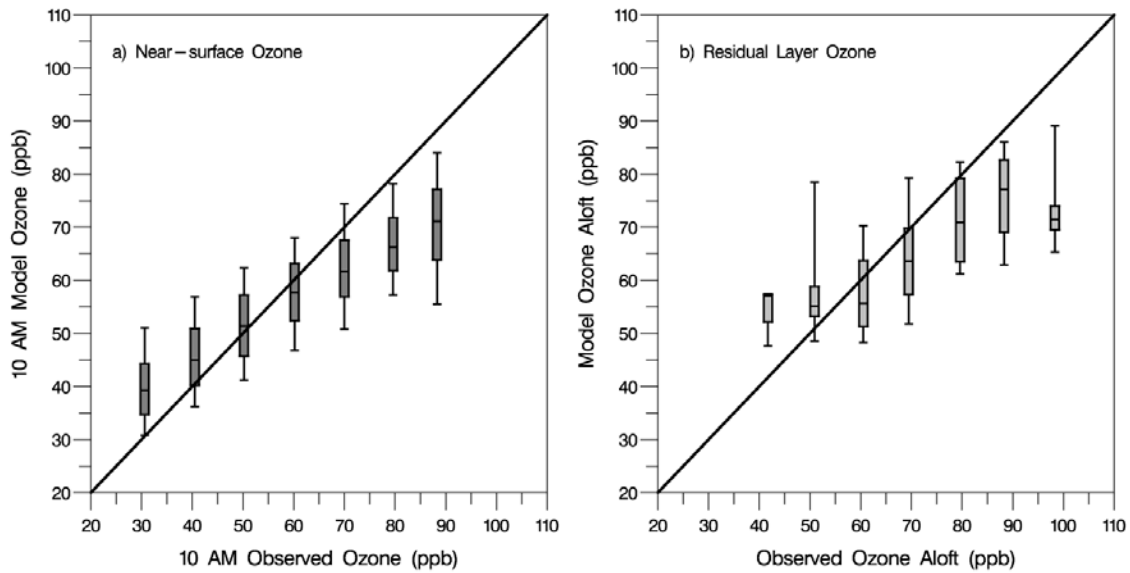


Figure 3. a) Modeled ozone concentrations at 10 AM versus observed 10 AM ozone levels from rural eastern surface AQS sites during summer 2002 ozone episode days and b) modeled residual layer ozone versus observed residual layer ozone levels from UM aircraft profiles obtained during summer 2002 experimental days. The box/whisker results depict values at the median (line inside the boxes), box edges denote the 25th and 75th percentiles and whiskers extend to the 10th and 90th percentiles.

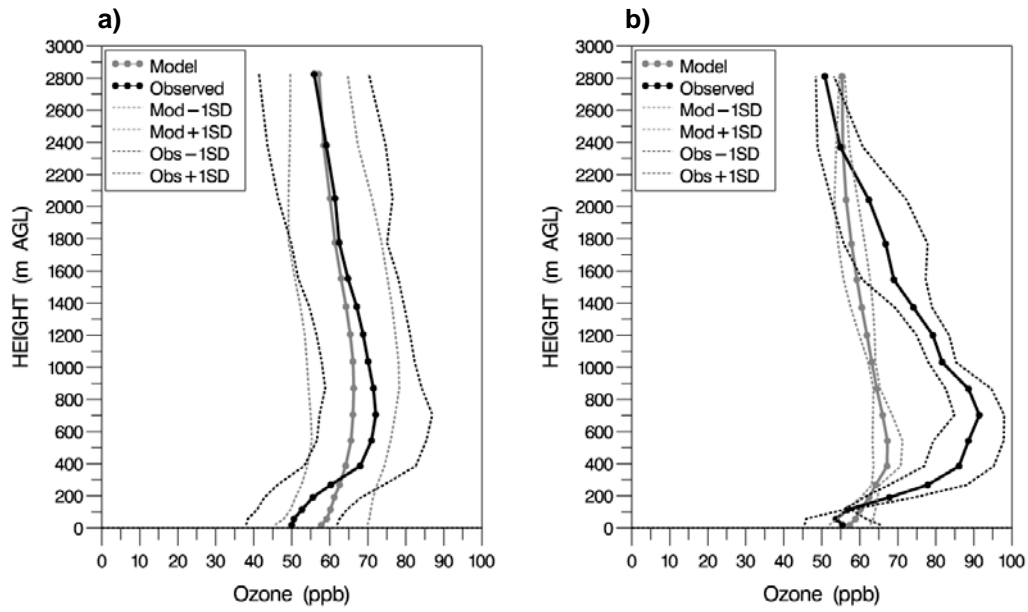


Figure 4. Mid-morning average modeled and observed UM aircraft ozone profiles a) from all sites in the mid-Atlantic region during June/July 2002 experimental cases and b) from 3 sites in VT/NH during August 13, 2002. The dashed lines represent ± 1 standard deviation (SD) from the average values.

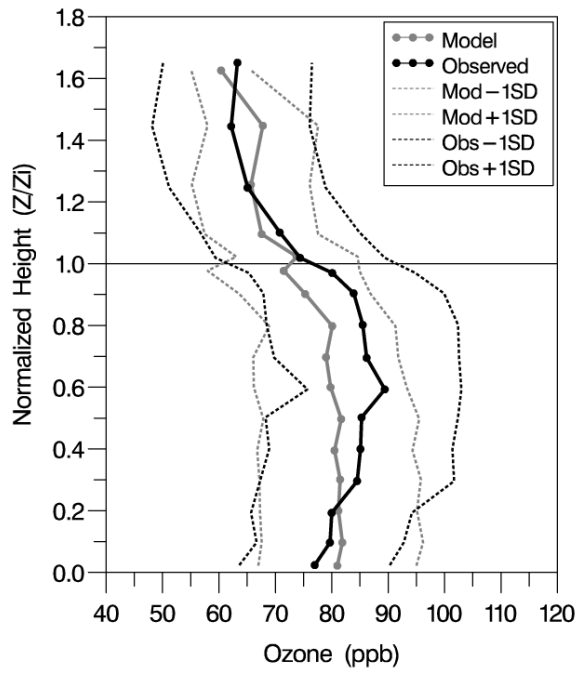


Figure 5. Modeled and UM aircraft average ozone profiles from mid-Atlantic and New England locations from mid-afternoon periods during summer 2002 episode cases. Height (z) is normalized by the PBL height (z_i). The dashed lines represent concentrations at ± 1 standard deviation (SD) from the average values.

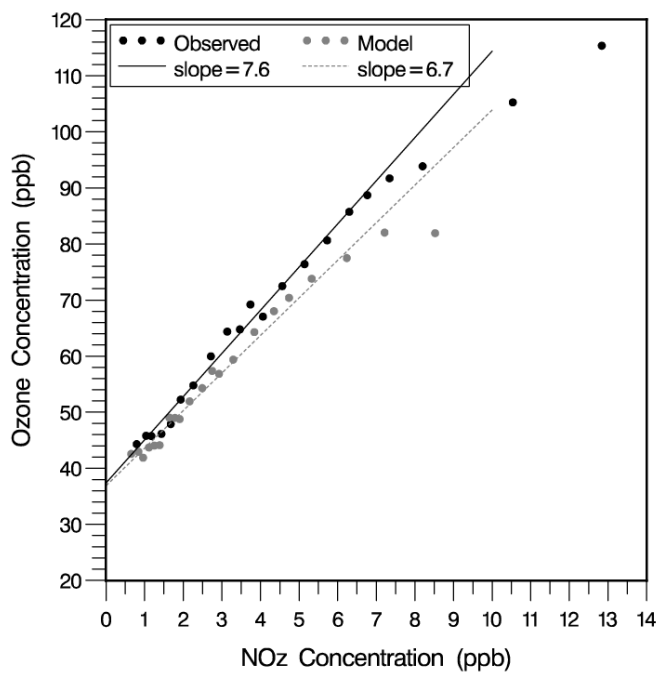


Figure 6. Relationship between ozone and NO_z from model results and BNL aircraft measurements along horizontal traverses near the middle of the PBL in the mid-afternoon during summer 2002 field study days. Lines depict linear regression fit to the modeled and observed results for NO_z values ≤ 8 ppb. Each symbol is derived from groups of values over 5% intervals of the observed and modeled concentration distributions.

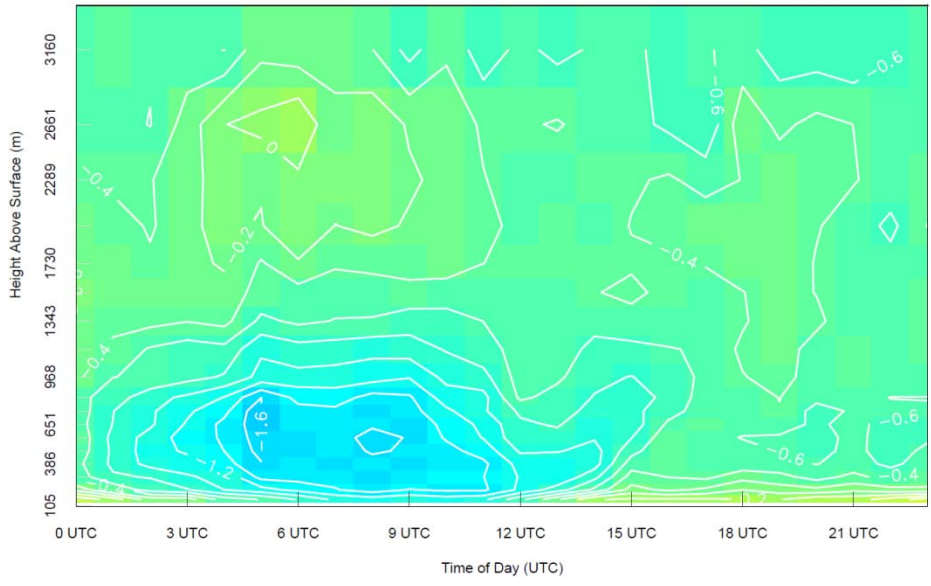


Figure 7. Vertical time section of the average wind speed difference (modeled – observed) over the diurnal cycle based on modeled and observed profiles from all eastern radar wind profiler sites during the summer 2002 period. Isopleths are given in units of m/s.

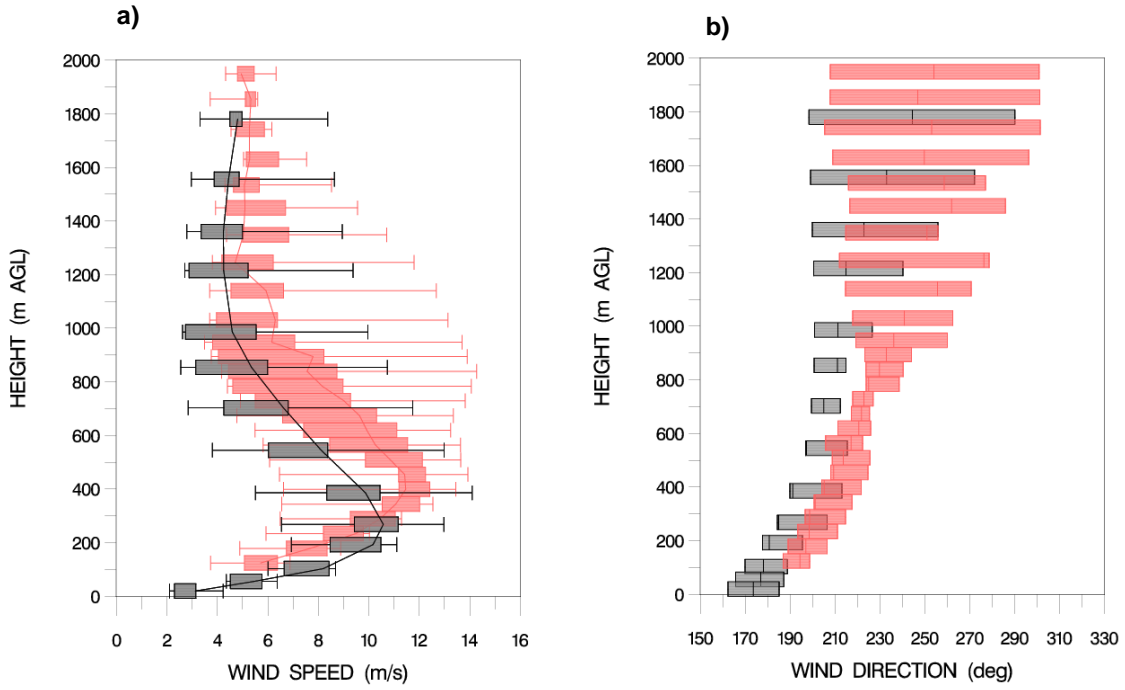


Figure 8. Modeled (gray) and observed (rose) a) wind speed and b) direction profiles averaged over the nocturnal periods of August 11-15, 2002 at Ft. Meade, MD. Boxes span the 25th to 75th percentiles, and whiskers in a) extend from 10th to 90th percentiles.

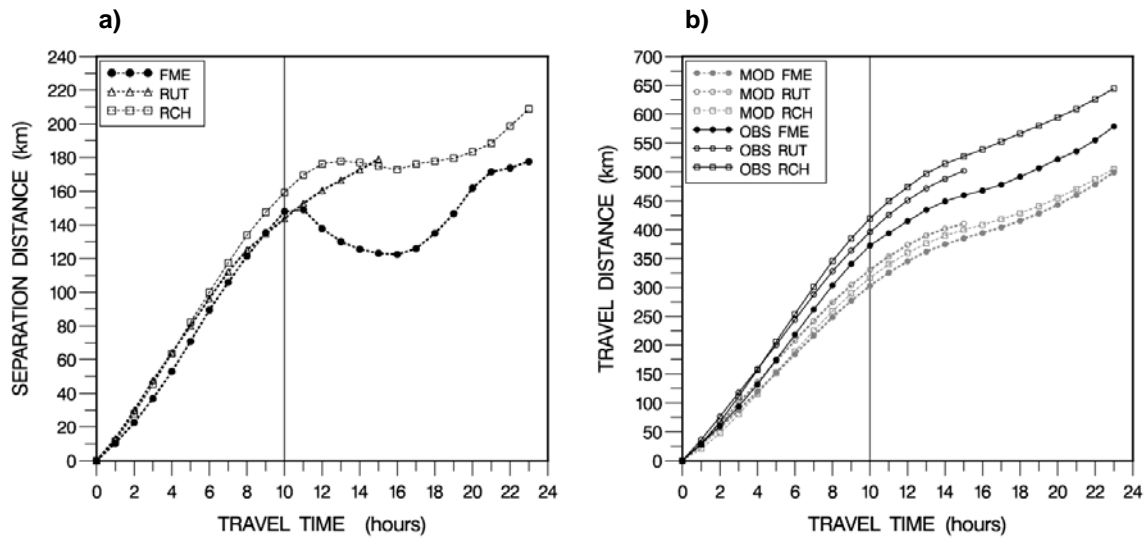


Figure 9. a) Spatial separation between modeled (with base FDDA) and observed forward trajectory positions with time and b) total travel distance of the trajectories based on hourly modeled and observed winds averaged over the August 2002 episode days. A starting time of 00 UTC and a release height of 500 m AGL were used for each trajectory from FME (Ft. Meade, MD), RUT (New Brunswick, NJ), and RCH (Richmond, VA). The RUT trajectory is abbreviated since it reached the eastern model boundary.

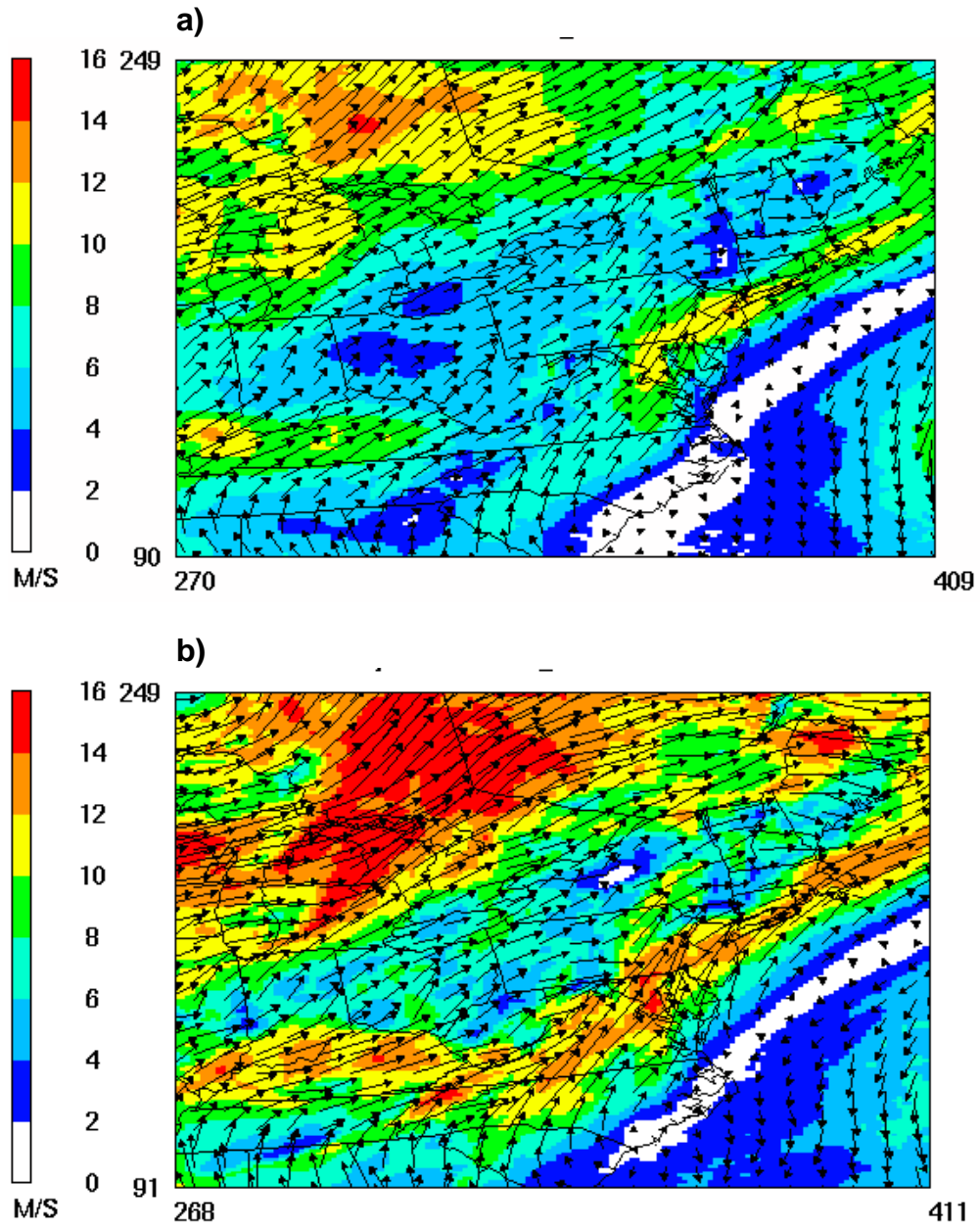


Figure 10. Wind flows depicting speeds (color tiles) and directions (arrows) near 500 m AGL at 0800 UTC on August 11, 2002 from WRF simulations with a) base FDDA and b) no FDDA below 2 km AGL.

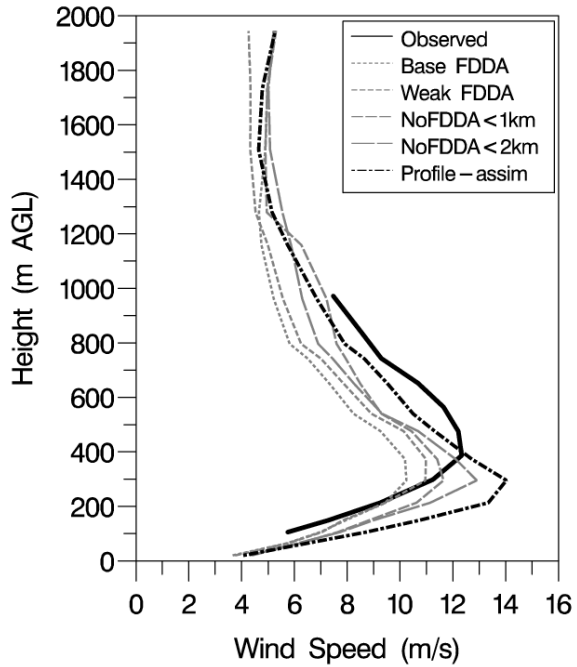
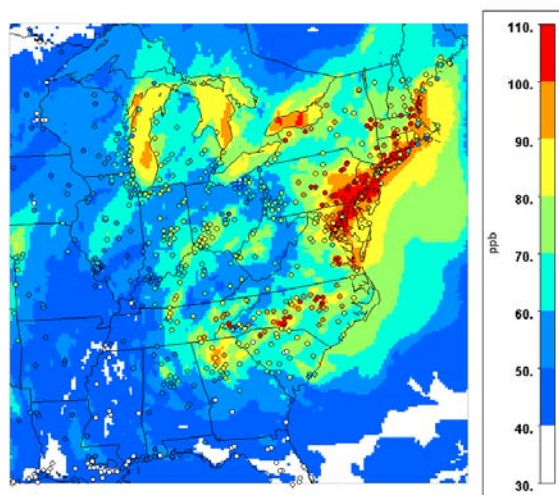


Figure 11. Modeled results averaged over the nocturnal period from different WRF simulations using different FDDA options versus an observed nocturnal average wind speed profile at Ft. Meade, MD from August 11, 2002. The observed profile has been truncated near 1000 m since profile data above this level were not available during all hours.

a)



b)

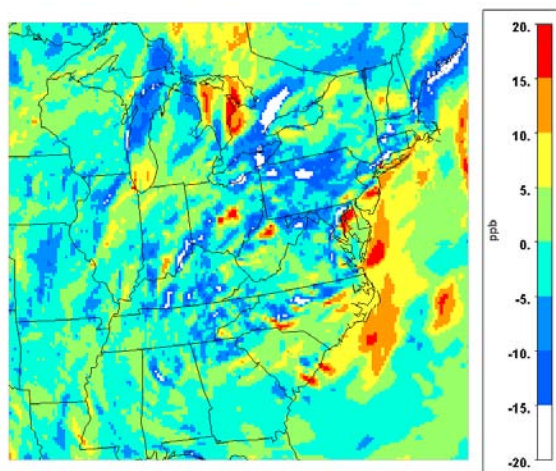
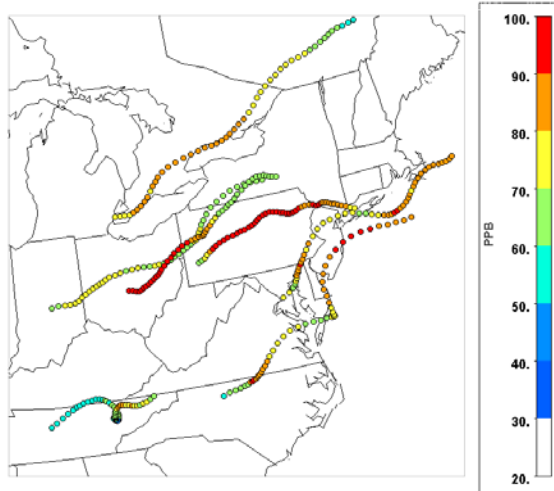


Figure 12. a) Modeled maximum 8-h O₃ field using improved wind fields (SENS9) on August 12, 2002 and AQS site values (circles), and b) differences in maximum 8-h O₃ (SENS9 - base) results.

a)



b)

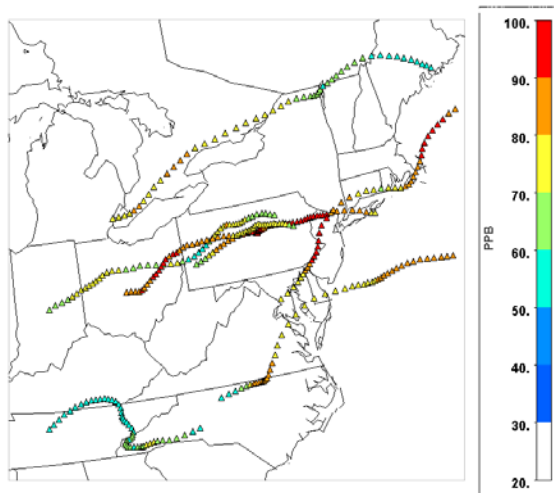
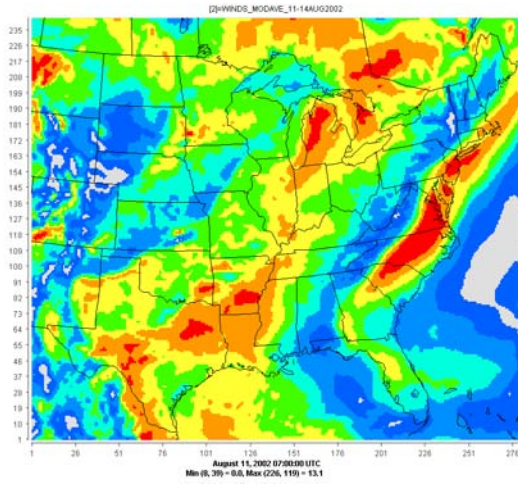


Figure 13. Ozone from CMAQ runs is depicted along the paths of forward trajectories released at 500 m AGL on August 11, 2002 starting at 1100 UTC and traveling for 50 hours downwind of select locations using a) base case and b) SENS9 sensitivity run wind fields.

a)



b)

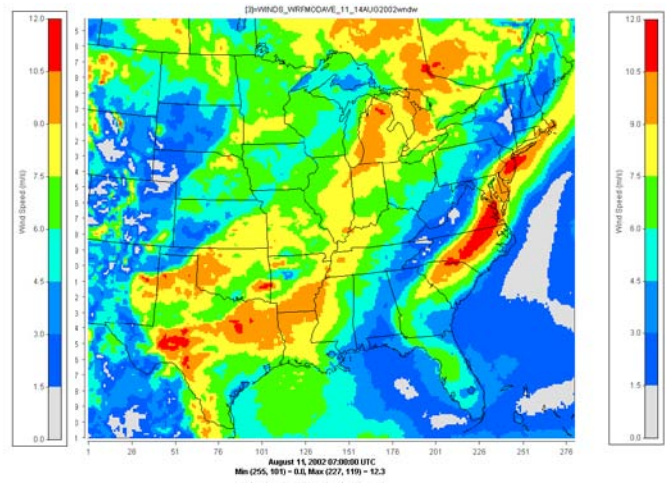


Figure A1. Wind speed fields on August 11, 2002 at 0700 UTC in layer 5 (≈ 300 m AGL) from FDDA base case simulations with the a) MM5 and b) WRF meteorological models.

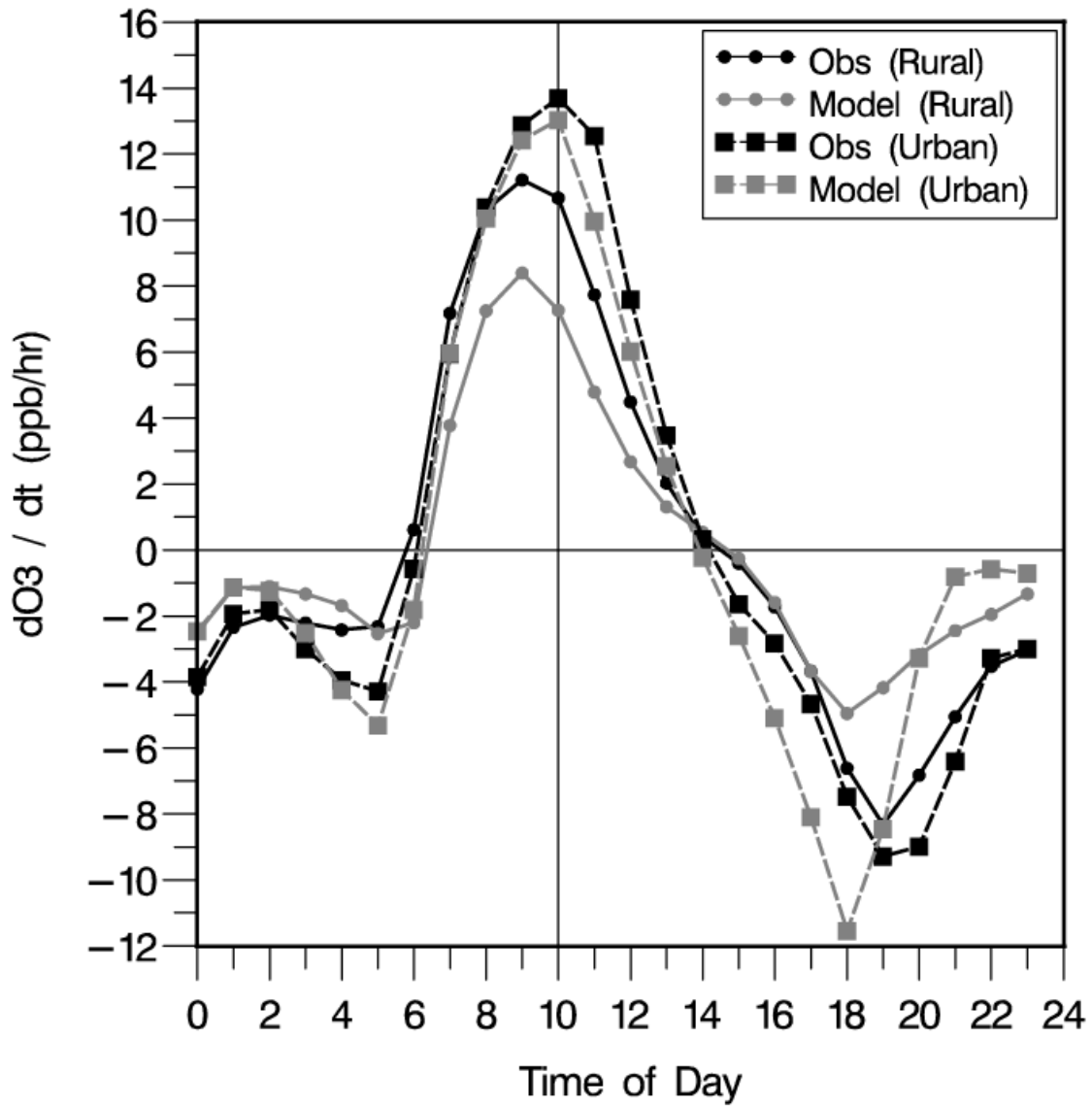


Figure A2. Hourly rate of change in ozone concentration at rural and urban AQS sites (black) and paired modeled results (gray) from episode days during summer 2002. The vertical line denotes 10 AM local time when the nocturnal inversion layer is often completely eroded and chemical production of ozone begins to be a greater contributor to increasing the ozone concentration.

Table A1. Observed Nocturnal Jet Peak Speed and Associated Characteristics versus Model Results at Ft. Meade, MD from the August 2002 episode days

Day	JD	Profiler Observations				Model* Results		
		Hr (UTC)	Z (m AGL)	Peak WS (m/s)	WD (deg)	Z (m AGL)	WS (m/s)	WD (deg)
11	223	08	454.	15.3	225.	386.	11.7	211.
12	224	06	454.	14.9	232.	268.	10.2	205.
13	225	05	344.	9.7	224.	193.	7.6	197.
14	226	06	729.	16.9	234.	386.	9.6	198.
15	227	05	783.	18.3	228.	386.	13.9	201.

* Results from MM5 base simulation with FDDA used in the CMAQ simulations

[11]=profiler10_0811_08UTC (OBS) [7]=WINDS_WRF34basefdda_11AUG2002t08 [8]=profiler_DATArev0811_08UTC (OBS)

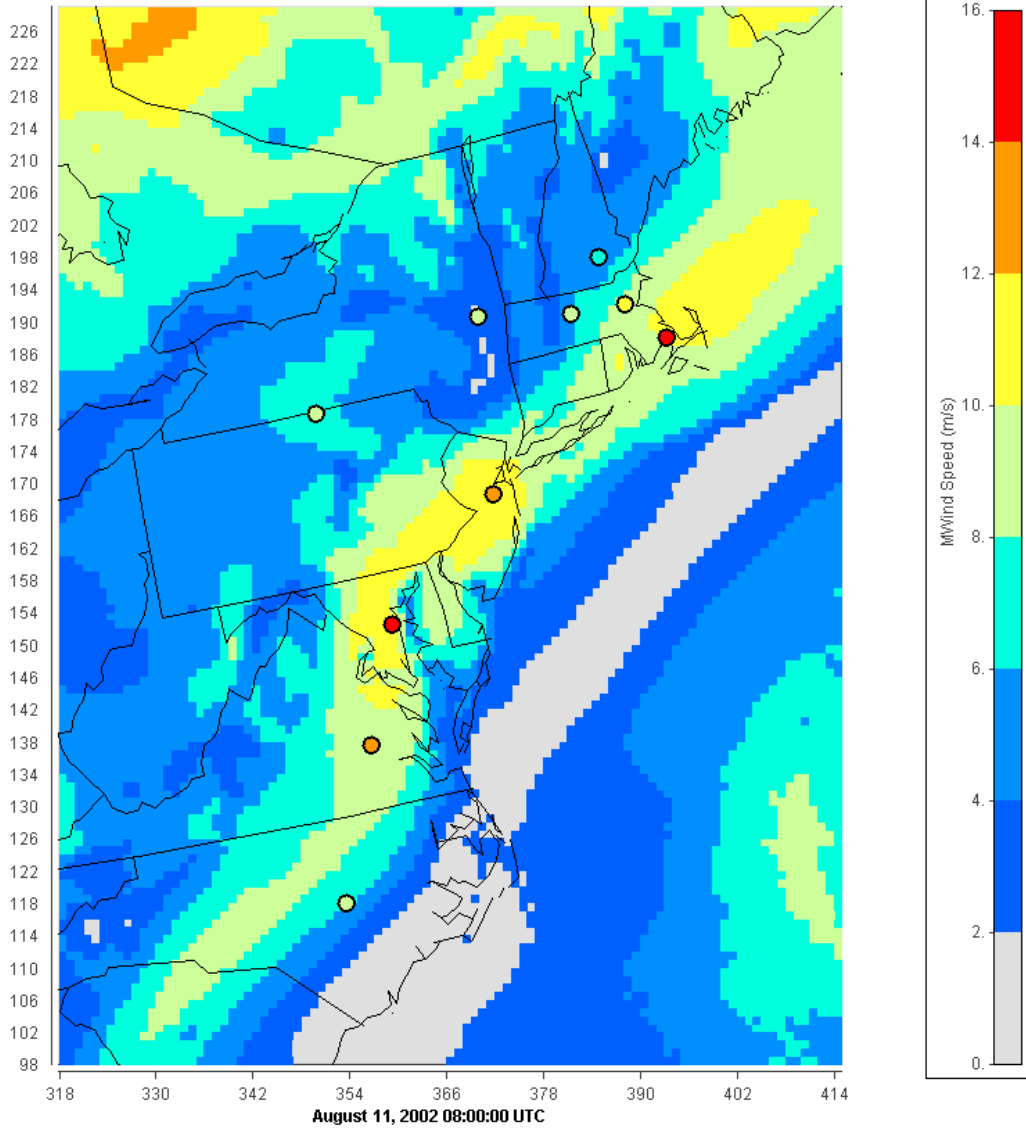


Figure A3. Model (base case) wind speed on August 11, 2002 at 300 m (layer 5) at 08 UTC and observed wind speeds at the same height from profiler sites.

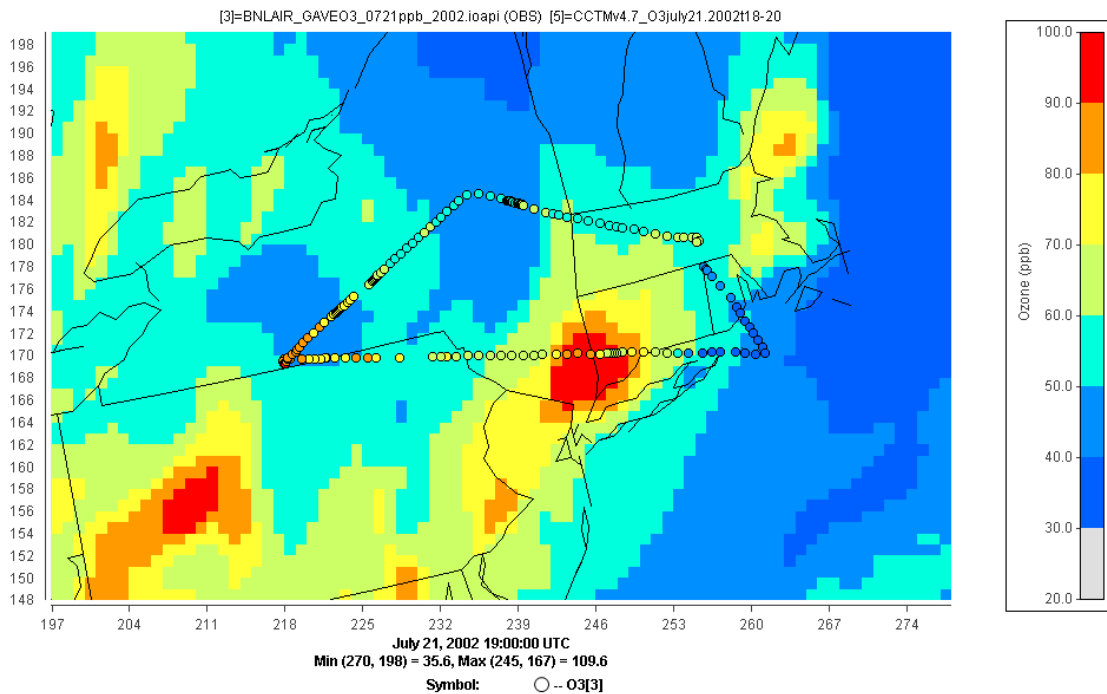


Figure A4. CMAQ ozone field and observed ozone along the BNL aircraft horizontal traverse in The northeastern US at 1900 UTC on July 21, 2002. Underestimated model winds caused the high ozone pattern in western PA to be several hours slow in arriving in the area of the flight path in elevated ozone along the NY/PA border, while the modeled high ozone area in the NY Hudson Valley/ western CT should be situated in central CT indicating modeled speeds were biased low.

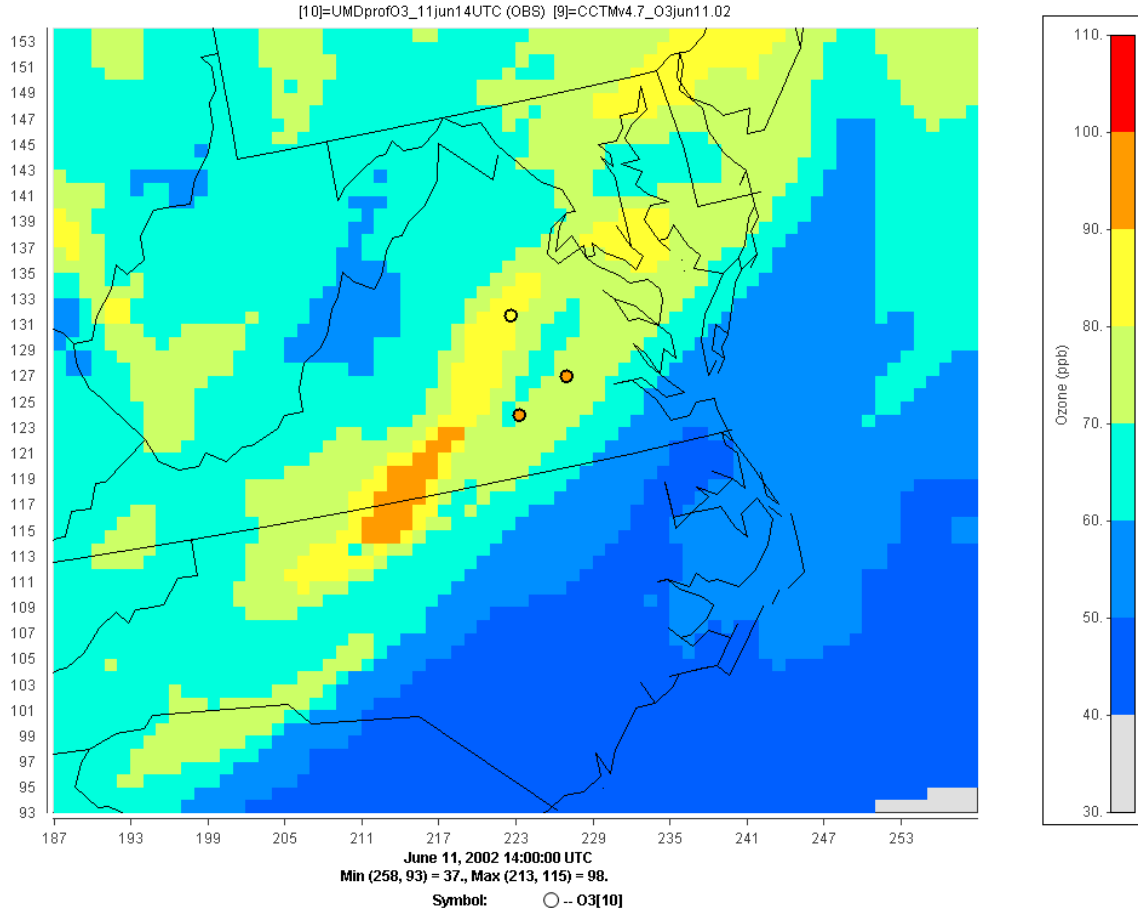


Figure A5. Another example of spatial displacement of the modeled ozone pattern versus observed ozone from vertical profiles of the UM aircraft in the Richmond, VA area in the mid-morning of June 11, 2002. Comparisons of modeled and observed wind profiles from the nocturnal period indicated the modeled wind speeds at this level (layer 7 ~ 400 m AGL) underestimated observed winds causing the high ozone area along the VA/NC border to be slow in arriving in the Richmond, VA area where the profiles were made.

Selected FDDA sensitivity runs with the WRF model are defined below with the results shown in the following supplemental figures.

Sensitivity Case Definition List

Base: surface nudging and 3-D OA nudging of winds above PBL
SENS3: no surface nudging or 3-D nudging below 2000 m
SENS5: no surface nudging and no u,v nudging in PBL
SENS6: no surface nudging and no u,v nudge in PBL + 500 m
SENS7: no surface nudging, spectral nudging with 250 km filter applied
SENS8: profiler data assimilated, with no surface nudging and no 3-D PBL nudging
SENS9: all wind profiles included (profiler sites, VAD radar profiles, and rawinsondes)
SENS10: SENS5, except with 47 layers
SENS11: lowest nudging level set at 1000 m, except when PBL height is greater, then lowest nudging level is set to PBL + 1 level.

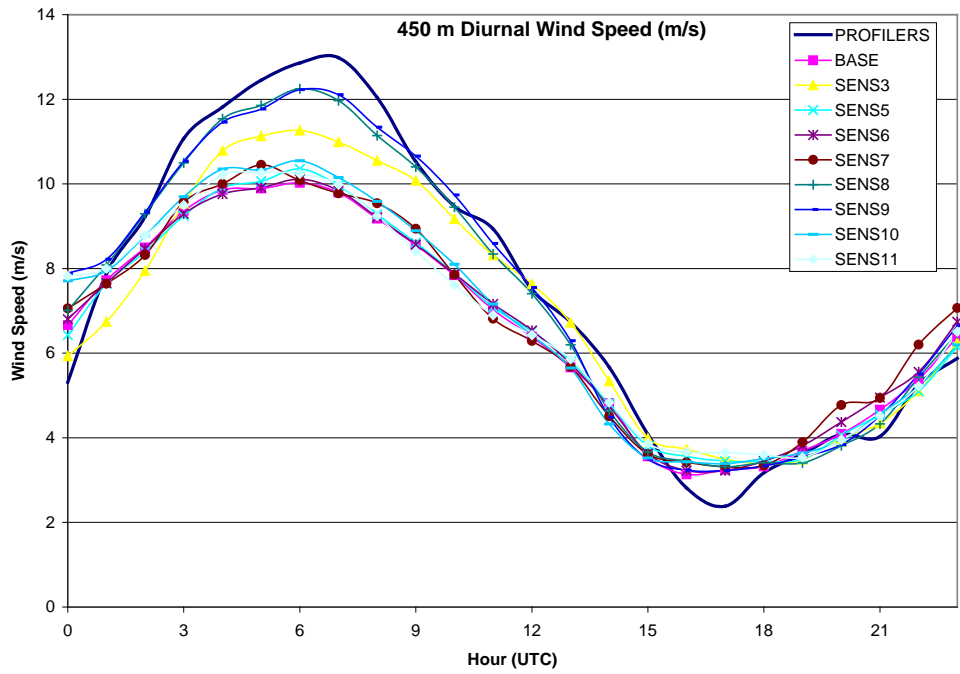
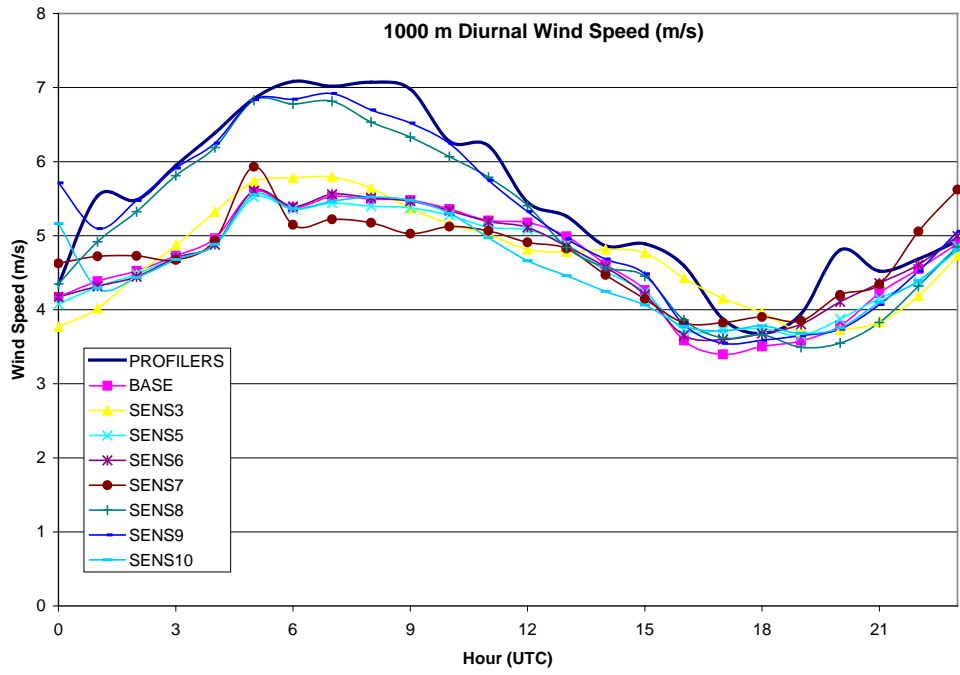


Figure A6. Modeled wind speed results from WRF simulations using different FDDA optional procedures compared to observed wind speeds from 4 mid-Atlantic profiler sites at 450 m AGL (bottom) and 1000 m AGL (top).

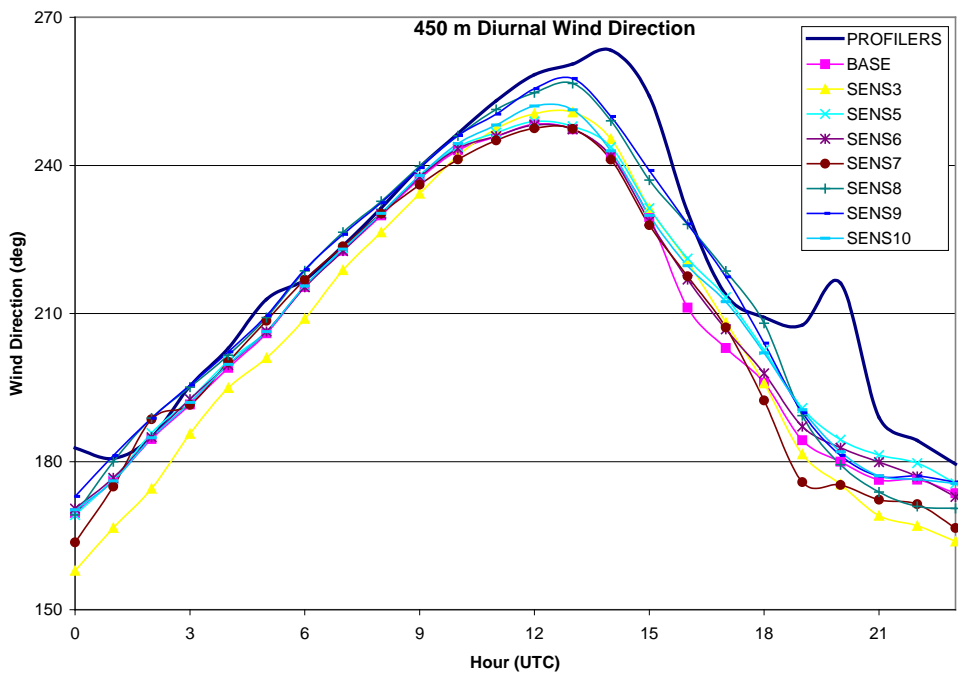
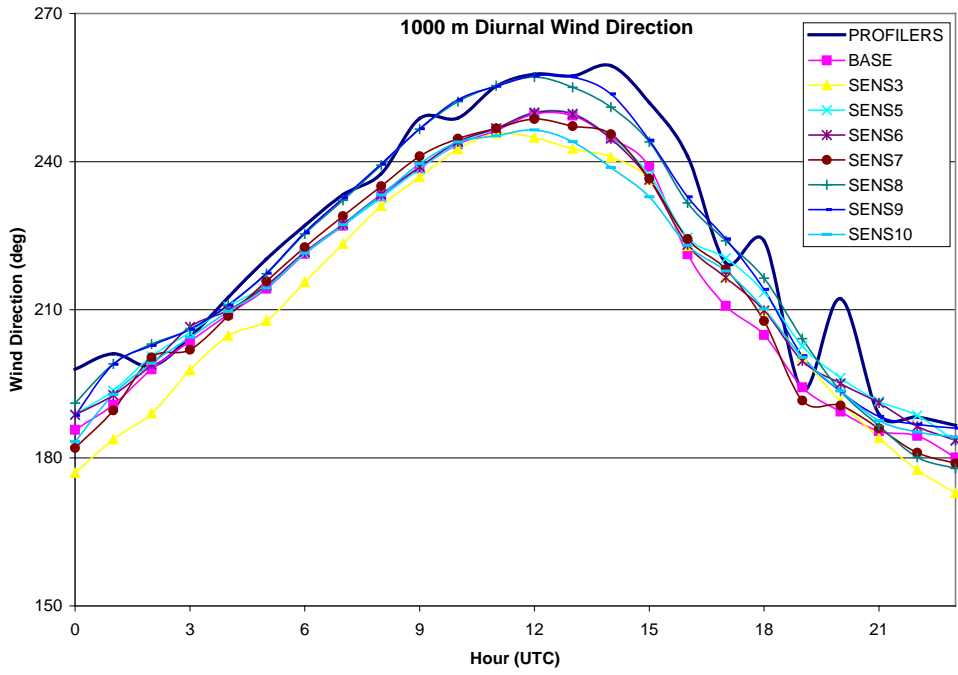


Figure A7. Modeled wind direction results from WRF simulations using different FDFA optional procedures compared to observed directions from 4 mid-Atlantic wind profiler sites at 450 m AGL (bottom) and 1000 m AGL (top).

